Ultra-wideband circular-polarization converter with micro-split Jerusalem-cross metasurfaces*

Xi Gao(高喜)[1,2,†], Xing-Yang Yu(余行阳)[1], Wei-Ping Cao(曹卫平)[1], Yan-Nan Jiang(姜彦南)[1], and Xin-Hua Yu(于新华)[1]

[1] School of Information and Communication, Guilin University of Electronic Technology, Guilin 541004, China
[2] Guangxi Key Laboratory of Wireless Wideband Communication & Signal Processing, Guilin 541004, China

(Received 7 June 2016; revised manuscript received 22 July 2016; published online 25 October 2016)

An ultrathin micro-split Jerusalem-cross metasurface is proposed in this paper, which can efficiently convert the linear polarization of electromagnetic (EM) wave into the circular polarization in ultra-wideband. By symmetrically employing two micro-splits on the horizontal arm (in the *x* direction) of the Jerusalem-cross structure, the bandwidth of the proposed device is significantly extended. Both simulated and experimental results show that the proposed metasurface is able to convert linearly polarized waves into circularly polarized waves in a frequency range from 12.4 GHz to 21 GHz, with an axis ratio better than 1 dB. The simulated results also show that such a broadband and high-performance are maintained over a wide range of incident angle. The presented polarization converter can be used in a number of areas, such as spectroscopy and wireless communications.

Keywords: circular-polarization converter, micro-split Jerusalem-cross metasurface, ultrathin, ultra-wideband

PACS: 81.05.Xj, 41.20.Jb **DOI:** 10.1088/1674-1056/25/12/128102

1. Introduction

Polarization is one of the fundamental properties of electromagnetic (EM) waves. Many applications and optical devices, such as liquid crystal displays, microwave communications and polarization converters are inherently sensitive to polarization, and hence full control of the polarization states of the EM waves is highly desirable. Conventional polarization-manipulation devices are usually realized by utilizing birefringence behaviors in crystals. In this way, polarization changes are obtained by phase accumulation when the EM waves propagate along the optical components, which leads to thick and bulky configurations in the devices.[1,2] Therefore, it is extremely inconvenient to integrate within ultrathin devices, such as nano-photonic devices and advanced sensors.

Metasurfaces are periodic or quasi-periodic planar arrays of sub-wavelength elements, which can be made on an ultrathin dielectric plate or optical thin film. They have received much attention since they offer reduced losses and lower profiles, and hence are simpler to fabricate than bulk metamaterials.[3,4] When the EM waves irradiate the metasurface, the desired phase discontinuity can be achieved by engineering the geometric parameters of the subwavelength elements such as the shape, size and orientation, yielding anomalous reflections and refractions.[5,6] Owing to such fascinating phenomena, metasurfaces break their dependences on the propagation effect by introducing abrupt changes of optical properties. Hence, many novel physical effects have been presented, such as photonic spin Hall effect,[7] beam focusing,[8] surface plasmon couplers,[9] three-dimensional computer-generated holography image reconstruction, and flat lenses.[10]

Recently, metasurfaces have been employed to manipulate the polarization states of the EM waves. By controlling the amplitudes and phases of the reflected or transmitted waves, many polarization converters have been successfully investigated and demonstrated.[11–20] In reflective linear polarization converters, the electric (symmetric mode) and magnetic (asymmetric mode) plasmonic resonances appear simultaneously.[21] The multi-resonant features can effectively extend the bandwidth. For example, by combining a cut-wire array with a ground metal plane, a broadband terahertz linear polarization converter with an efficiency of up to 80% in a frequency range between 0.8 THz and 1.36 THz has been successfully realized.[22] At microwave frequencies, a double V-shaped metasurface can rotate the linearly polarized wave into the cross-polarized one in an ultra-wideband (from 12.4 GHz to 27.9 GHz) with an over 90% polarization conversion efficiency.[23] As for the linear-to-circular polarization conversion, ultrathin quarter-wave plates based on metasurfaces have also been widely demonstrated.[24–28] However, these polarization devices have the obvious disadvantage of narrow bandwidth, which restricts the practical applications.

Here, we propose an ultra-wideband linear-to-circular po-

*Project supported by the National Natural Science Foundation of China (Grant Nos. 61461016 and 61661012), the Natural Science Foundation of Guangxi Zhuang Autonomous Region, China (Grant Nos. 2014GXNSFAA118366, 2014GXNSFAA118283, and 2015jjBB7002), and the Innovation Project of Graduate Education of Guilin University of Electronic Technology, China (Grant No. 2016YJCX82).

†Corresponding author. E-mail: gao_xi76@163.com

© 2016 Chinese Physical Society and IOP Publishing Ltd

larization converter based on an ultrathin metasurface that is composed of micro-split Jerusalem-cross structures. We show that by employing two narrow slits on the horizontal arms, we can significantly expand the bandwidth of the linear-to-circular polarization converter. Both numerical simulation and experiment results show that the polarization converter can convert the linearly polarized wave into the circularly polarized wave in an ultra-wideband from 12.4 GHz to 21 GHz, and the fractional bandwidth with an axial ratio better than 1 dB reaches 50%. Moreover, its broadband polarization conversion performance is supported in a wide range of incident angles, providing the convenience in practical applications.

2. Design and results

The reflection polarization converter is usually made up of a metasurface and a continuous metallic ground spaced by a dielectric plate, in which the metasurface formed by a periodic array of unit cells with an asymmetric structure is considered as an anisotropic homogeneous material with dispersive relative permittivity and permeability. When a plane wave with specified polarization irradiates the polarizer, the reflected EM wave can be decomposed into two perpendicular components which are denoted as $\boldsymbol{E}_r = \boldsymbol{E}_{rx} + \boldsymbol{E}_{ry} = E_x \mathrm{e}^{\mathrm{j}\varphi_x}\boldsymbol{x} + E_y \mathrm{e}^{\mathrm{j}\varphi_y}\boldsymbol{y}$. Owing to the anisotropic characteristics of the metasurface, the two components $\boldsymbol{E}_{rx}$ and $\boldsymbol{E}_{ry}$ have different amplitudes and phases, which determine the polarization characteristics of the reflected EM wave. By choosing an adaptive metasurface unit cell and an appropriate thickness of the dielectric plate, so that $\boldsymbol{E}_{rx}$ and $\boldsymbol{E}_{ry}$ have the same amplitude and phase difference of $2n\pi \pm \pi/2$ (n is an integer), a circular polarization reflected wave is thus realized.

According to the principles described above, we design a micro-split Jerusalem-cross metasurface that can convert linear polarization of the EM wave into circular polarization in an ultra-wide band. The proposed polarization converter is formed by a micro-split Jerusalem-cross metasurface and a metallic ground spaced by an ultrathin dielectric plate as illustrated in Fig. 1. The metasurface admittance is equal to a sheet admittance which is capacitive in the x direction and inductive in the y direction. The admittance values make sure that there is 90° phase difference between the x and y polarized refection waves. Furthermore, the micro-splits etched in the I-shaped arm in the x direction can maintain the 90° phase difference in an ultra-wide band, which dramatically extends the band width of the proposed polarizer. The unit cell and its geometrical dimensions are illustrated in Fig. 1(b), in which $L_1 = 4.1$ mm, $L_2 = 2.9$ mm, $L_3 = 2.4$ mm, $w_1 = 0.3$ mm, $w_2 = 0.5$ mm, and $r = 0.75$ mm. The width of micro-split and the periodicity of the metasurface structure are set to be $g = 0.15$ mm and $p = 5$ mm, respectively. The metallic layer is modeled as a copper film with a thickness of 0.035 mm and an electrical conductivity $\sigma = 5.8 \times 10^7$ S/m. The dielectric layer is selected as F4B with a relative permittivity of 2.65, loss tangent of 0.001, and thickness $d = 2.5$ mm.

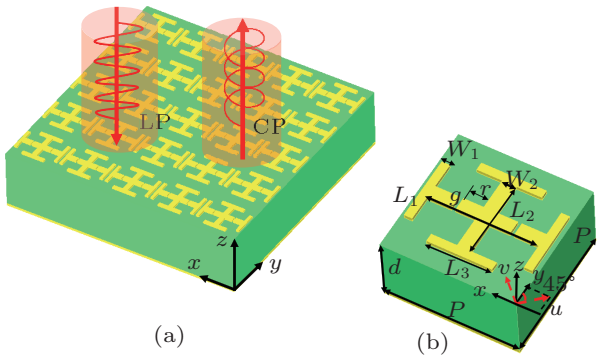


Fig. 1. (color online) (a) Schematic of linear-to-circular polarization conversion. (b) A unit cell of the proposed polarizer.

We implement three-dimensional (3D) full wave simulations using commercial software CST Microwave Studio to verify the performance of the ultra-wideband linear-to-circular polarization converter. In simulations, a single unit cell with periodic boundary condition along the x and y direction is employed, and a plane wave with electric field polarized along the u direction (45° relative to the x axis, see Fig. 1(b)) impinging on the unit cell is used as an excitation source. Due to the anisotropic characteristics of the metasurface, both u and v polarized reflection waves are generated. We define R_{uu} and R_{vu} to denote the reflection coefficients of the u and v polarized reflective waves, respectively. The simulated results are illustrated in Figs. 2(a) and 2(b), from which we can clearly see that the reflections of the two orthogonal reflective waves are almost equal, and their phase difference $\Delta\varphi_{vu}$ ($\Delta\varphi_{vu} = \arg(R_{vu}) - \arg(R_{uu})$) is equal to $-270°$ in a frequency range from 12.4 GHz to 21 GHz. It implies that the linearly-polarized incident wave is converted into the circularly-polarized wave in this ultra-wideband frequency range.

In order to obtain a further insight into the performance of the proposed circular polarization converter, we introduce the Stokes parameters as follows:[13]

$$S_0 = |R_{uu}|^2 + |R_{vu}|^2, \quad S_1 = |R_{uu}|^2 - |R_{vu}|^2,$$
$$S_2 = 2\,|R_{uu}|\,|R_{vu}|\cos\Delta\varphi_{vu}, \quad S_3 = 2\,|R_{uu}|\,|R_{vu}|\sin\Delta\varphi_{vu}. \quad (1)$$

Then, we define the normalized ellipticity as $e = S_3/S_0$ to descript the circular polarization ability. When $e = 1$, the reflected wave is a left-handed circularly-polarized (LHCP) wave; when $e = -1$, the reflected wave is a right-handed circularly-polarized (RHCP) wave. According to Eq. (1), we can obtain the ellipticity of the proposed circular polarization

converter by using the simulated and experimental reflection coefficients and phase difference shown in Figs. 2(a) and 2(b), and the results are illustrated in Fig. 2(c). It is clearly seen that the ellipticity is nearly equal to 1 in a frequency range from 12.4 GHz to 21 GHz, implying an LHCP conversion in an ultra-wideband. The electric fields at different phases distributed (see the inset in Fig. 2(c)) on unit cell show obviously counter-clockwise rotation, which also demonstrates the characteristic of LHCP. Figure 2(d) gives the axial ratios of reflected waves, from which we observe that the axial ratio is less than 1 dB in the same frequency range as ellipticity $e = 1$. Figures 2(c) and 2(d) demonstrate the excellent performance of the proposed circular-polarization converter in ultra-wideband.

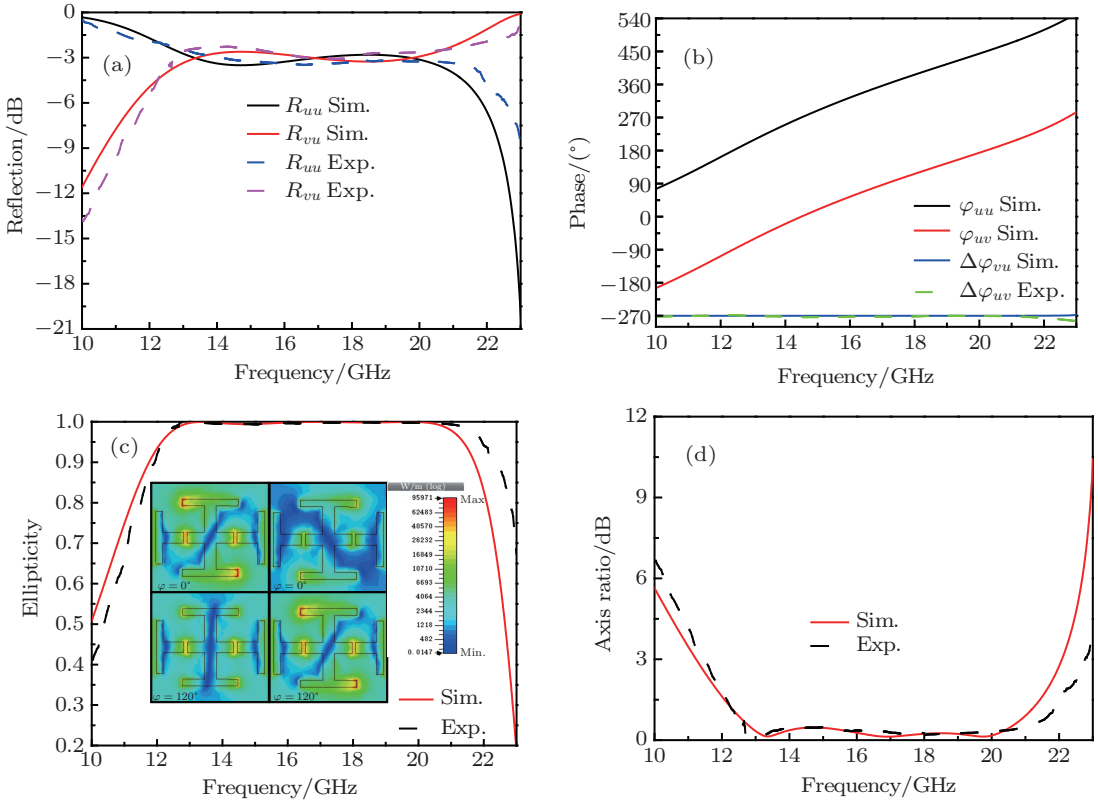


Fig. 2. (color online) Performance of the proposed circular polarization converter, in which the dashed lines are experimental results and the solid lines correspond to simulation results. (a) Reflections for the co-polarized and cross-polarized wave at normal incidence. (b) Phases of reflection coefficients R_{uu} and R_{vu} and their phase differences. (c) Normalized ellipticities of the reflected waves. (d) Axial ratios.

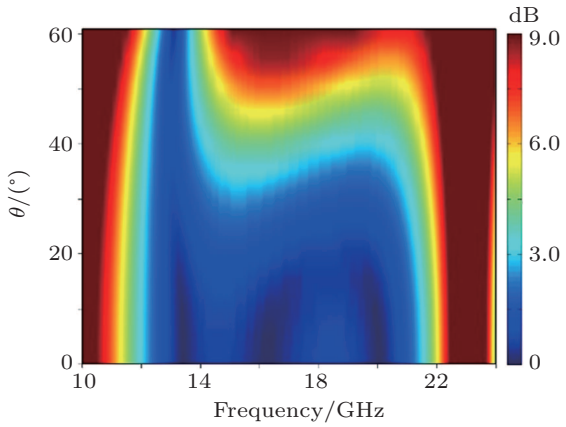


Fig. 3. (color online) Simulated axial ratio of the designed polarization converter as a function of the incident angle θ and frequency.

An interesting characteristic of the proposed circular polarization converter is that it can maintain the excellent performance of circular polarization for a large incident angle. Figure 3 gives the axial ratios of reflected wave for different incident angles. It is clearly seen that the axial ratios are less than 2 dB in the ultra-wideband from 12.4 GHz to 21 GHz when the incident angle changes from 0° to 35°. However, when the incident angle is greater than 35°, the circular polarization bandwidth sharply decreases with incident angle decreasing. The characteristic of wide incident angle makes the circular polarization converter very convenient in practical application.

3. Physical mechanism

Here, we investigate electromagnetic (EM) response of the proposed metasurface based on an equivalent circuit theory. The proposed metasurface can be modeled as a series *LC* circuit,[29] in which the capacitor *C* results from the electric field distribution in the gaps between metallic wires, and the inductor *L* is related to the current distribution on the metallic wires and decreases with their lengths and widths.[30] To demonstrate it, we observe the surface currents and electric

field distributions at four typical frequencies corresponding to 13, 15, 18, and 21 GHz when the y and x polarized waves are normally incident on the metasurface, respectively. The observed results are shown in Figs. 4 and 5, respectively. Figure 4 shows the current distributions, from which we clearly see that the surface currents distribute on the I-shaped arm in the y direction, implying the inductive characteristic. Meanwhile in Fig. 5, we find that the electric field concentrates on the micro-splits and the gaps between the I-shaped arms along the x axis, demonstrating the capacitive property of these I-shaped arms.

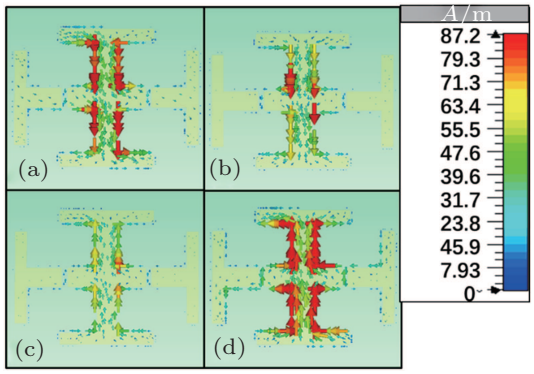


Fig. 4. (color online) Simulated surface current distributions on the cell of metasurface for the y-polarized incident wave at frequencies of (a) 13 GHz, (b) 15 GHz, (c) 18 GHz, and (d) 21 GHz.

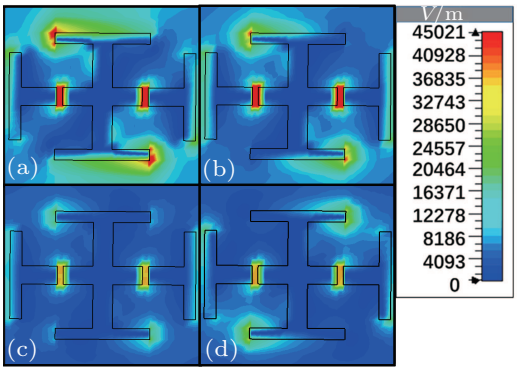


Fig. 5. (color online) Simulated surface electric field distributions on the cell of metasurface for x-polarized wave. (a) 13 GHz, (b) 15 GHz, (c) 18 GHz, and (d) 21 GHz.

In order to further study the EM response of the proposed metasurface, we first consider the Jerusalem-cross array without ground and dielectric substrate. Then it can be modeled as a two-port network as shown in Fig. 6(a). The air around the Jerusalem-cross array is considered as an equivalent transmission line with characteristic impedance Z_0, while the Jerusalem-cross array is replaced by a series LC circuit which is parallel connected with the equivalent transmission line. So the equivalent circuit of the metasurface is obtained as shown in Fig. 6(b).

The characteristic of the equivalent two-port network can be analyzed by using the following transfer matrix:

$$\begin{pmatrix} A & B \\ C & D \end{pmatrix} = \begin{pmatrix} A_1 & B_1 \\ C_1 & D_1 \end{pmatrix} \begin{pmatrix} A_2 & B_2 \\ C_2 & D_2 \end{pmatrix} \begin{pmatrix} A_1 & B_1 \\ C_1 & D_1 \end{pmatrix}$$

$$= \begin{pmatrix} 1 & Z_0 \\ 0 & 1 \end{pmatrix} \begin{pmatrix} 1 & 0 \\ \mathrm{j}\omega L_{\mathrm{eff}} + \dfrac{1}{\mathrm{j}\omega C_{\mathrm{eff}}} & 1 \end{pmatrix} \begin{pmatrix} 1 & Z_0 \\ 0 & 1 \end{pmatrix}, \quad (2)$$

where $\begin{pmatrix} A_1 & B_1 \\ C_1 & D_1 \end{pmatrix}$ and $\begin{pmatrix} A_2 & B_2 \\ C_2 & D_2 \end{pmatrix}$ are transfer matrices of the free space and the Jerusalem-cross array, ω is the angular frequency, Z_0 is the characteristic impedance of equivalent transmission line, and the L_{eff} and C_{eff} are equivalent capacitive and inductance of I-shaped arms.

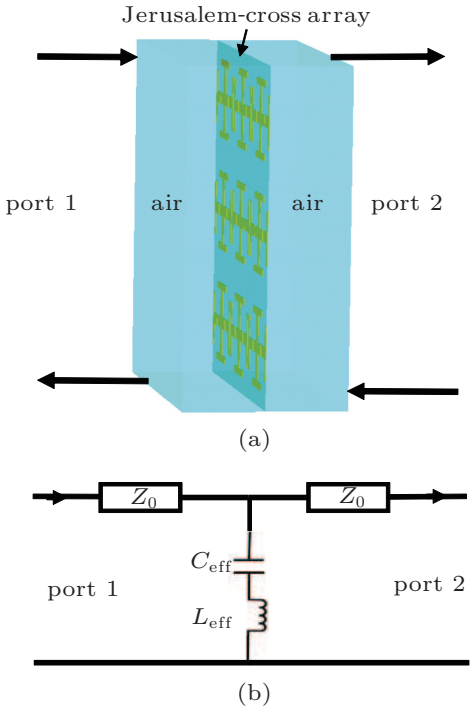


Fig. 6. (color online) (a) Equivalent two-port network of the free-standing Jerusalem-cross array. (b) Circuit model of the equivalent cascaded two-port networks.

If we transform the $ABCD$ matrix of the whole network into S-parameters matrix as

$$\begin{pmatrix} S_{11} & S_{12} \\ S_{21} & S_{22} \end{pmatrix} = \begin{pmatrix} \dfrac{B/Z_0 - CZ_0}{A + B/Z_0 + CZ_0 + D} & \dfrac{2}{A + B/Z_0 + CZ_0 + D} \\ \dfrac{2}{A + B/Z_0 + CZ_0 + D} & \dfrac{B/Z_0 - CZ_0}{A + B/Z_0 + CZ_0 + D} \end{pmatrix}, \quad (3)$$

then the phase of the transmitted wave can be solved as

$$\begin{aligned} \phi &= \arg\left(\frac{2}{A + B/Z_0 + CZ_0 + D}\right) \\ &= a\tan\left(Z_0\left(\frac{1}{\omega C_{\mathrm{eff}}} - \omega L_{\mathrm{eff}}\right)\right), \end{aligned} \quad (4)$$

where

$$a = 1/(1 + z_0^2(\omega^2 L_{\mathrm{eff}}^2 + 1/\omega^2 C_{\mathrm{eff}}^2 - 2L/C)).$$

For the y-polarized incident wave, the transmitted wave is mainly related to the inductive effect of the I-shaped arms in

the y direction (see Fig. 4). Therefore the transmission phase ϕ_y is determined by the inductance L_{eff} and denoted as

$$\phi_y = a\tan(-Z_0\omega L_{\text{eff}}). \tag{5}$$

Correspondingly, for the x-polarized incident wave, the transmitted wave is mainly related to the capacitance effect of the I-shaped arms in the x-direction (see Fig. 5). So the transmission phase ϕ_x is approximately denoted as

$$\phi_x = a\tan\left(\frac{Z_0}{\omega C_{\text{eff}}}\right). \tag{6}$$

When a u-polarized wave is incident on the Jerusalem-cross array, it can be decomposed into$x$- and y-polarized components. Based on the aforementioned theory, the phase of transmitted waves in the x and y direction are respectively related to the capacitance (C_{eff}) and the inductance (L_{eff}) of the equivalent series LC circuit. Furthermore, the inductive element results in phase delay of y-polarized component, and the capacitance leads to the phase advance of the x-polarized component.[31] Then a phase difference between x and y electric field components can be obtained as

$$\Delta\phi = \phi_y - \phi_x = a\left(\tan\left(-Z_0\omega L_{\text{eff}}\right) - \tan\left(\frac{Z_0}{\omega C_{\text{eff}}}\right)\right). \tag{7}$$

It should be noted that the C_{eff} and L_{eff} are affected by the dimension parameters or the configurations of the I-shaped arms in the x and y directions. It provides us a method to obtain the prescribed phase difference ($\Delta\phi$) by changing the parameters and configurations of the I-shaped arms in the x and y directions. Here we obtain the desired phase by symmetrically employing micro-split in the I-shaped arms along the x-direction and optimizing their parameters.

On the other hand, when a metallic ground plane is placed on the other side of the dielectric substrate, the transmitted waves are totally reflected. Hence, an incident wave that illuminates the metasurface undergoes multiple reflections and transmissions between the metasurface and metallic ground, where they interfere with another one to create the final reflected wave.[32] So the dielectric thickness is another critical parameter to affect the phase of the wave transmitting in the dielectric substrate, implying that a dispersion-free broadband polarization converter can be realized by carefully choosing the thickness of dielectric substrate.

In order to study the physical mechanism in more detail, we study the reflection characteristics by using the multiple reflection interference theory and the physical model is shown in Fig. 7(a). Assuming that the incident electric field is $\boldsymbol{E}_{\text{in}}$, the total reflected electric field is then calculated by superposition of all multiple reflections as follows:[32]

$$R = \frac{\boldsymbol{E_r}}{\boldsymbol{E_{in}}} = \tilde{r}_{12} - \frac{\tilde{t}_{12}\tilde{t}_{21}\,\mathrm{e}^{\mathrm{j}2kd}}{1+\tilde{r}_{21}\,\mathrm{e}^{\mathrm{j}2kd}}, \tag{8}$$

where r_{12}, r_{21}, t_{12}, and t_{21} are the reflection and transmission coefficients at the interface of metastructure (see Fig. 7(a)), k is the transmission constant in the dielectric substrate, and d is the distance between the metasurface and ground plane. The r_{12}, r_{21}, t_{12}, and t_{21} can be calculated by CST Microwave Studio.

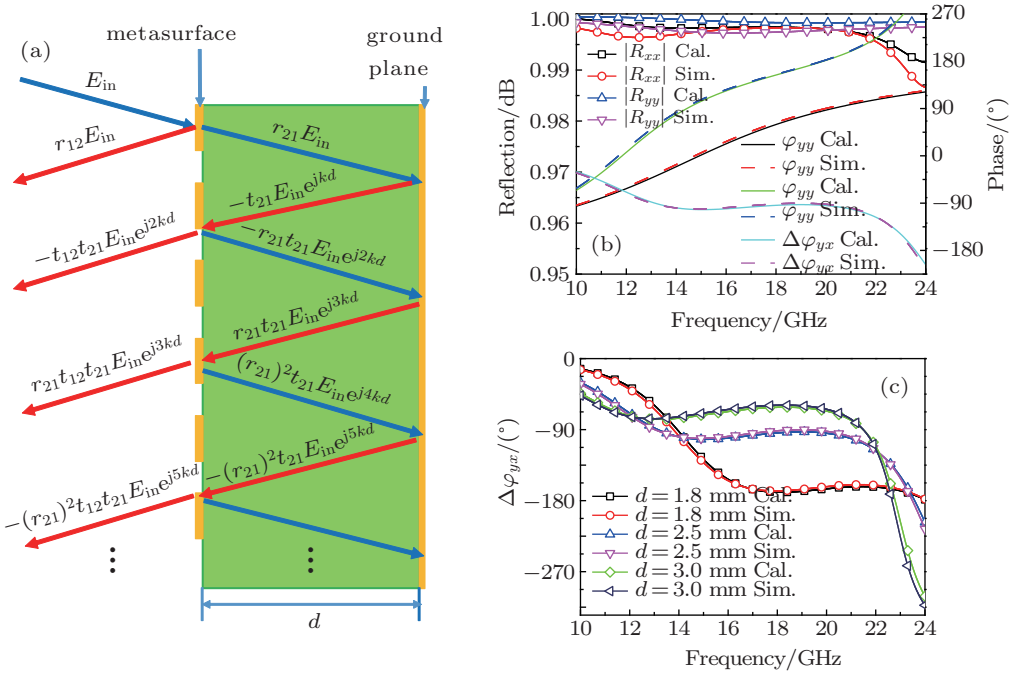


Fig. 7. (color online) (a) Model of multiple reflections and transmissions for the reflective metasurface, (b) calculated and simulated reflection coefficients of x- and y-polarized reflected waves, and (c) dispersion curves of phase difference between x- and y-polarized reflected waves for different values of dielectric thickness.

According to Eq. (8), when the x- and y-polarized waves respectively illuminate the polarization converter, the calculated reflection coefficients of R_{ii} $(i = x, y)$ are shown in Fig. 7(b), in which R_{ii} denotes the reflection coefficient of i-polarized reflective wave for i-polarized incident wave. For comparison, we also give the simulated results. From Fig. 7(b), we can observe that the theoretical results are in good agreement with the simulated ones. Furthermore, we also find that $|R_{xx}|$ is equal to $|R_{yy}|$ and the phase difference $\Delta\varphi_{yx}(\arg(R_{yy}) - \arg(R_{xx}))$ is equal to $-90°$ in the frequency range from 12.4 GHz to 21 GHz. It implies that when a u-polarized wave (E_{iu}) which can be equally decomposed into two components (E_{ix} and E_{iy}) is incident on the polarization converter, an ultra-wideband linear-to-circular polarization conversion can be realized as shown in Fig. 2. We also study the influence of dielectric thickness on $\Delta\varphi_{yx}$, which is shown in Fig. 7(c). It can be seen that only when $d = 2.5$ mm, the $\Delta\varphi_{yx}$ is approximately equal to 90°, implying the possibility of realizing circular polarization conversion.

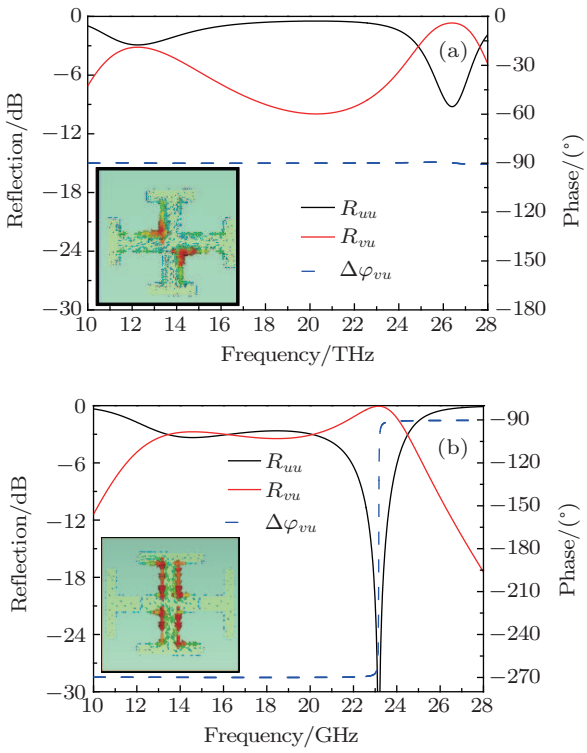


Fig. 8. (color online) Comparison of performance of circular polarization conversion between the converter consisting of conventional Jerusalem-cross metasurface (a) and the proposed converter (b). The inserts are the distributions of surface current on metasurface.

We also compare the performance of the proposed polarization converter with the one consisting of Jerusalem-cross without micro-split (conventional Jerusalem-cross) as illustrated in Fig. 8. In order to obtain linear-to-circular polarization, the parameters of the Jerusalem-cross should be slightly modified when the micro-splits are moved away. The optimized parameters are set to be $L_1 = 3.6$ mm, $L_2 = 2.9$ mm, $L_3 = 1.6$ mm, $w_1 = 0.35$ mm, $w_2 = 0.5$ mm, $p = 5$ mm, and $d = 2.5$ mm (see Fig. 1(b)). As we can see from Fig. 8, the circular polarization bandwidth for conventional Jerusalem-cross is in the frequency range from 11.5 GHz to 13.5 GHz. It implies that the operation bandwidth is dramatically reduced when the micro-splits are moved out from the I-shaped arms in the x-direction. The inserts in Figs. 8(a) and 8(b) show the surface currents distributed on normal Jerusalem-cross and micro-split Jerusalem-cross, respectively. For normal Jerusalem-cross, the surface currents are equivalently distributed on the arms in the x and y directions, whereas for the micro-split Jerusalem-cross, most of the surface currents are distributed only on the arms in the y direction. Therefore, when micro-splits are etched on the I-shaped arms in the x direction, their admittances are changed from inductive to capacitive ones. As discussed previously, the alternative admittance greatly improves the performance of circular polarization converter.

4. Experimental verification

To experimentally validate the proposed polarization converter, the metasurface is fabricated on the F4B substrate by using the conventional printed circuit board (PCB) technique as shown in Fig. 9(a). The configuration for fabrication has an overall size of 250 mm × 250 mm, containing 50 × 50 unit cells. In measurement, a network analyzer (Agilent 8753ES) is used, whose two ports are connected to two identical horns. The fabricated sample is placed on the front of the horn antennas and surrounded by absorbing materials (see the Fig. 9(b)). The 1# horn is employed to emit the horizontally-polarized incident waves, and the 2# horn is a received horn by which the magnitudes of the horizontally- and vertically-polarized reflected waves (that is R_{uu} and R_{vu}) can be obtained. To ensure that the sample receives and reflects the EM waves, the sample and horn antennas are kept at the same height. On the other hand, the phases of R_{uu} and R_{vu} are very sensitive to the wave path since our polarization converter operates at higher frequencies. Consequently, it is very difficult to obtain the precise phase difference ($\Delta\varphi_{uv}$) by using the measured phase data of R_{uu} and R_{vu}. In order to obtain the precise phase difference, we rotate the 2# antenna to the 45° polarization to receive the corresponding amplitude of the reflected wave $|R_{xu}|$ (see the inset in Fig. 9(b)). Then, the phase difference $\Delta\varphi_{vu}$ can be calculated from the following equations:[33]

$$|R_{xu}|^2 = \frac{|R_{vu}|^2}{2} + \frac{|R_{uu}|^2}{2} + |R_{vu}|\,|R_{uu}|\cos\Delta\varphi_{vu}, \quad (9)$$

$$\cos\Delta\phi_{vu} = \frac{2\,|R_{xu}|^2 - |R_{uu}|^2 - |R_{vu}|}{2\,|R_{uu}|\,|R_{vu}|}. \quad (10)$$

In experiments, we consider only the case of normal incidence. The measured $|R_{uu}|$ and $|R_{vu}|$, and the phase difference $\Delta\varphi_{vu}$ are represented by dashed lines in Figs. 2(b) and 2(c). The axis ratio is denoted as dashed lines in Fig. 2(d). It

is clearly seen that the experimental results show good agreement with numerical simulations, demonstrating the high performance of the proposed circular-polarization converter.

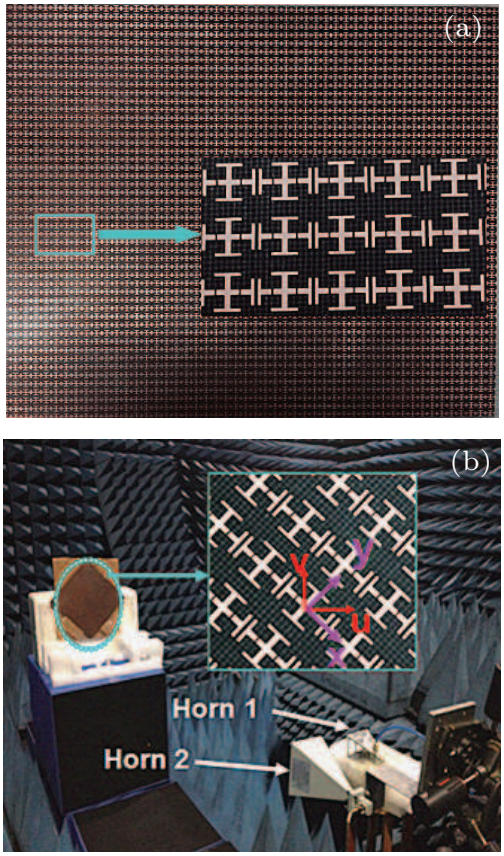


Fig. 9. (color online) Images of the fabricated sample (a) and experimental setup (b).

5. Conclusions

We present an ultra-wideband and high-performance circular-polarization converter by using ultrathin micro-split Jerusalem-cross metasurface. Numerical simulation and measurement results demonstrate that the proposed design can convert the linearly-polarized EM wave to circularly-polarized wave in a frequency range of 12.4 GHz–21 GHz, with a fractional bandwidth of 50%. Furthermore, the ultra-wideband polarization conversion performance is maintained in a wide range of incident angles. We also investigate the physical mechanism by using the equivalent circuit method. The proposed polarization converter will have many potential applications at the microwave and terahertz frequencies.

References

[1] Stalder M and Schadt M 1996 *Opt. Lett.* **21** 1948
[2] Heismann F and Aferness R 1988 *IEEE J. Quantum Electron.* **24** 83
[3] Yu J B, Ma H, Wang J F, Li Y F, Feng M D and Qu S B 2015 *Chin. Phys. B* **24** 098102
[4] Yan X, Liang L J, Zhang Y T, Ding X and Yao J Q 2015 *Acta Phys. Sin.* **64** 0158101 (in Chinese)
[5] Yu N, Genevet P, Kats M A, Aieta F, Tetienne J P, Capasso F and Gaburro Z 2011 *Science* **334** 333
[6] Yu N and Capasso F 2014 *Nat. Mater.* **13** 139
[7] Yin X B, Ye Z L, Rho J, Wang Y and Zhang X 2013 *Science* **339** 1405
[8] Li X, Xiao S Y, Cai B G, He Q, Cui T J and Zhou L 2012 *Opt. Lett.* **37** 4940
[9] Lin J, Mueller J B, Wang Q, Yuan G, Antoniou N, Yuan X C and Capasso F 2013 *Science* **340** 331
[10] Aieta F, Genevet P, Kats M A, Yu N, Blanchard R, Gaburro Z and Capasso F 2012 *Nano Lett.* **12** 4932
[11] Shi J H, Liu X C, Yu S W, Lv T T, Zhu Z, Ma H F and Cui T J 2013 *Appl. Phys. Lett.* **102** 191905
[12] Ding F, Wang Z X, He S L, Shalaev V M and Kildishev A V 2015 *ACS Nano* **9** 4111
[13] Chen H Y, Wang J F, Ma H, Qu S B, Xu Z, Zhang A X, Yan M B and Li Y F 2014 *J. Appl. Phys.* **115** 154504
[14] Shi J H, Ma H F, Guan C Y, Wang Z P and Cui T J 2014 *Phys. Rev. B* **89** 165128
[15] Cong L Q, Xu N N, Gu J Q, Singh R, Han J G and Zhang W L 2014 *Laser Photon. Rev.* **8** 626
[16] Ma X L, Cheng H, Pu M B, Hu C G, Qin F and Luo X G 2012 *Opt. Express* **20** 16050
[17] Yu N, Aieta F, Genevet P, Kats M A, Gaburro Z and Capasso F 2012 *Nano Lett.* **12** 6328
[18] Cheng H, Chen S Q, Yu P, Li J X, Xie B Y, Li Z C and Tian J G 2013 *Appl. Phys. Lett.* **103** 223102
[19] Liu W W, Chen S Q, Li, Z C, Cheng H, Yu P, Li J X and Tian J G 2015 *Opt. Lett.* **40** 3185
[20] Wu J L, Lin B Q and Da X Y 2016 *Chin. Phys. B* **25** 088101
[21] Dong G X, Shi H Y, Xia Y, Li W, Zhang A X, Xu Z and Wei X Y 2016 *Chin. Phys. B* **25** 084202
[22] Grady N K, Heyes J E, Chowdhury D R, Zeng Y, Reiten M T, Azad A K, Taylor A J and Chen H T 2013 *Science* **340** 1304
[23] Gao X, Han X, Cao W P, Li H O, Ma H F and Cui T J 2015 *IEEE Trans. Antenn. Propag.* **63** 3522
[24] Wang D C, Gu Y H, Gong Y D, Qiu C W and Hong M H 2015 *Opt. Express* **23** 11114
[25] Huang X J, Yang D and Yang H L 2014 *J. Appl. Phys.* **115** 103505
[26] Zhu H, Cheung S W, Chung K L and Yuk T I 2013 *IEEE Trans. Antenn. Propag.* **61** 4615
[27] Cheng H, Chen S Q, Yu P, Li J X, Deng L and Tian J G 2013 *Opt. Lett.* **38** 1567
[28] Li Z C, Liu W W, Cheng H, Chen S Q and Tian J G 2015 *Sci. Rep.* **5** 18106
[29] Pfeiffer C and Grbic A 2014 *Phys. Rev. Appl.* **2** 044011
[30] Guo Y H, Wang Y Q, Pu M B, Zhao Z Y, Wu X Y, Ma X L, Wang C T, Yan L S and Luo X G 2015 *Sci. Rep.* **5** 8434
[31] Ma X L, Huang C, Pu M B, Hu C G, Feng Q and Luo X G 2012 *Microw. Opt. Techn. Lett.* **54** 1770
[32] Chen H T 2012 *Opt. Express* **20** 7165
[33] Jiang S C, Xiong X, Hu Y S, Hu Y H, Ma G B, Peng R W, Sun C and Wang M 2014 *Phys. Rev. X* **4** 021026